Nanopore Direct RNA Sequencing Reveals Virus-Induced Changes in the Transcriptional Landscape in Human Bronchial Epithelial Cells

Dongyu Wang[a], J. Leland Booth[b], Wenxin Wu[b], Nicholas Kiger[a], Matthew Lettow[c], Averi Bates[d], Chongle Pan[a,d], Jordan Metcalf[b,e,f], Susan J. Schroeder[a,c]#

[a]School of Biological Sciences, University of Oklahoma, Norman, OK, USA

[b]Pulmonary, Critical Care & Sleep Medicine Section, Department of Medicine, University of Oklahoma Health Sciences Center, Oklahoma City, OK USA

[c]Department of Chemistry & Biochemistry, University of Oklahoma, Norman, OK, USA

[d]School of Computer Science, Gallogly College of Engineering, University of Oklahoma, Norman, OK, USA

[e]Department of Microbiology and Immunology, the University of Oklahoma Health Sciences Center, Oklahoma City, USA

[f]Veterans Affairs Medical Center, Oklahoma City, OK, USA

Running Head: Nanopore RNA Sequencing Transcriptional Landscape

#Address correspondence to Susan J. Schroeder, susan.schroeder@ou.edu

Key words: Direct RNA nanopore sequencing, m6A methylation, virus-host interaction, influenza infection in primary human bronchial epithelial cells, epitranscriptomics

Abstract

Direct RNA nanopore sequencing reveals changes in gene expression, polyadenylation, splicing, m6A methylation, and pseudouridylation in response to influenza virus exposure in primary human bronchial epithelial cells. This study focuses on the epitranscriptomic profile of genes in the host immune response. In addition to polyadenylated noncoding RNA, we purified and sequenced nonpolyadenylated noncoding RNA and observed changes in expression, N6-methyl-adenosine (m6A), and pseudouridylation (Ψ) in these novel RNA. Two recently discovered lincRNA with roles in immune response, *Chaserr* and *LEADR*, became highly methylated in response to influenza exposure. Several H/ACA type snoRNAs that guide pseudouridylation are decreased in expression in response to influenza, and there is a corresponding decrease in the pseudouridylation of two novel lncRNA. Thus, novel epitranscriptomic changes revealed by direct RNA sequencing with nanopore technology provides unique insights into the host epitranscriptomic changes in epithelial gene networks that respond to influenza virus infection.

Introduction

Seasonal influenza and pandemic influenza present significant health concerns. The Centers for Disease Control estimates that 9 million – 41 million illnesses, 140,000 – 710,000 hospitalizations and 12,000 – 52,000 deaths annually between 2010 and 2020 were due to influenza (1). Viruses are master manipulators of host cellular resources. Changes in ribonucleic acid (RNA) provide the genetic instructions for a host cell to respond to a virus infection. The changes in modified nucleotides can alter splicing and the way that the RNA folds and interacts with proteins and thus finetune host gene regulation responses to viruses. The epitranscriptome includes all the changes in modified nucleotides in response to cell stresses and developmental gene regulation. This manuscript presents a study of the transcriptomic and epitranscriptomic changes in response to influenza virus infection in primary human bronchial epithelial cells (HBEC) using direct RNA sequencing from Oxford Nanopore Technology and reveals changes in RNA abundance, nucleotide modifications, splicing isoforms, and polyA tail length in response to influenza. We identify changes in RNA methylations in both coding and noncoding RNA. Direct RNA nanopore sequencing (DRS) is a single molecule, long-read sequencing technology that measures nucleotide modifications, splicing isoforms, polyA tail length, and differential expression in a single assay. The method, therefore, demonstrates at higher resolution the changes in viral and host RNA that occur during IAV infection and host immune response, enhancing our understanding of these processes.

RNA adenosine methylation is an important regulatory mechanism of the transcriptional response to viral infection. N6-methyl-adenosine (m6A) is the most

common modified RNA nucleotide, and the levels of m6A change globally in response to many types of viral infections (2-5). m6A modifications regulate splicing(6), translational efficiency, RNA folding and tertiary interactions, RNA-protein interactions, and RNA cellular half-life in human transcriptomes (7-9). m6A modulates host response through several different gene networks. IAV infection induces a strong IFN immune response through Regulatory Transcription Factor (IRF) 7 activation in human lung bronchial and alveolar epithelial cell models (10). Adenosine methylation negatively regulates the type I interferon response through m6A modification of *IFNβ* mRNA in many kinds of viral infection, including influenza infection (11). The loss of m6A methylation on *IFNβ* mRNA increases mRNA stability and thus causes a more sustained IFN-β production and a more robust antiviral response. In Herpes Simplex Virus 1 infection, m6A methylation increases mRNA half-lives of the immune response genes *IFIH1*, *TNFIP3*, *IFIT1* and reduces the half-life of *IFIT2* mRNA (12). In Kaposi's sarcoma-associated herpesvirus infection, methylation of IL-6 transcripts in the 3'UTR recruit the YTHDC2 reader, preventing viral SOX-induced mRNA degradation (3), again increasing the half-life of this transcript. In adenovirus viral RNA transcripts, m6A methylation regulates the splicing efficiency of late-stage genes (13). In developing attenuated Respiratory Syncytial Virus (RSV) vaccines, RSV viral RNA that lacks m6A binds RIG-I with greater affinity, induces higher RIG-I expression and ubiquitination, increases IRF3 phosphorylation, increases RIG-I IFN signaling, and enables a higher IFN response (14). m6A methylation in the 3' UTR region can either stabilize or destabilize the cellular lifetime of the RNA transcript. For example, M6A in the 3'UTR and coding regions of *STAT1* increases the cellular stability of *STAT1*, a key master regulator of macrophage differentiation (15). In contrast, m6A methylation

of the 3'UTR in the *PTX3* gene increases the degradation of the RNA transcript and results in the repression of M2 activation (16). Previous studies have shown that m6A changes globally in response to virus infection (17, 18). Our data in HBEC cells uses direct RNA nanopore sequencing to identify these m6A changes in the context of full-length, single-molecule transcript reads revealing epitranscriptomic changes in the immune response gene network.

Traditional studies of RNA methylations in influenza infections have used mass spectrometry or variations of Illumina sequencing with m6A specific antibodies to pull down modified RNA fragments (9, 11, 19-23). Direct RNA sequencing with nanopore technology offers a new window to study RNA methylations directly in long sequencing reads. Nanopore sequencing technology uses a motor protein in a pore in a synthetic lipid bilayer to transfer a single molecule of DNA or RNA across a membrane. The voltage in picoamperes is measured as a function of time and sampled at 4 KHz. The voltage varies depending on the sequence of 5-6 nucleotides that are located in the channel of the pore and the corresponding pH difference on each side of the membrane. Modified nucleotides such as m6A alter the pK_a of the adenine base and correspondingly change the signal in the nanopore data. Modified nucleotides cause changes in the signal intensity, duration, and frequency of base calling errors (24, 25). m6Anet uses a multiple instance learning framework to analyze the nanopore signals to predict the probability and abundance of an m6A modified nucleotide at a specific nucleotide position in a transcript(26). m6Anet currently outperforms other analysis methods in accuracy (27).

Nanopore sequencing is currently being used to directly sequence and monitor influenza RNA. Oxford Nanopore Technology has developed ARTIC protocols to identify novel, emergent RNA viruses and new sequences of influenza viral RNA (28-31). The variations in m6A in influenza viral mRNA were first observed using RNA digestion and high pressure liquid chromatography (32). m6A methylation of some influenza viral transcripts enhances viral replication (21). More recently, nanopore sequencing of the influenza coding genome used specific adapter sequences to detect the viral RNA in cultured cells (33). Since the first application of Direct RNA Sequencing (DRS) to study influenza, significant improvements in basecalling software Guppy and Dorado (34) and identification of m6A using machine learning programs such as m6Anet have advanced nanopore DRS. Both host and viral RNA change methylations in response to virus infection (19). This nanopore DRS study focuses on the host immune response to viral exposure and the local and global changes in m6A methylation in coding and noncoding RNA. The study uses primary human airway epithelial cells to examine this process in a relevant human lung model of infection.

Materials and Methods

Cell culture. Human bronchial epithelial cells (HBEC) were collected from three clinical samples donated by healthy, adult non-smokers of diverse ages, genders, and races. All samples were collected following protocols that were approved by the Institutional Review Board of the University of Oklahoma Health Sciences Center (IRB # 2197). HBEC were obtained by bronchoscopy with bronchial brushing. Three or four separate third or fourth order bronchi are brushed and the cells are rinsed from the brush into 10 ml sterile saline until $5x10^6$ to $1x10^7$ cells total were collected as determined by

hemocytometer counts for total viable cells as assessed by trypan blue exclusion. The cells for isolation were resuspended to $5x10^5$ cells/ml in complete Bronchial Epithelial Cell Growth Medium (BEGM; Lonza Group Ltd.); were seeded into collagen coated tissue culture plates (Bio-Coat, BD Biosciences) at a density of $1x10^5$ cells/cm^2 and were propagated in an incubator at 37°C in 5% CO_2. After 24 h the cells are washed with HBSS to remove non-adherent cells and fresh complete BEGM is added. When the cultures are near confluence (7-10 days), the monolayers are lifted with 1x Accutase solution and are subcultured at a 1:5 dilution. After each passage the cells grow to confluence within 4 to 5 days, and when the cultures are split, freezer stocks are prepared in 80% BEGM + 10% fetal bovine serum + 10% DMSO and are stored at in liquid nitrogen vapor at -190°C.

HBEC infection, Virus stock preparation. The HBEC were infected with influenza as previously described(10, 35). H1N1 influenza A virus, A/PR/34/8 (PR8), was passaged in Madin-Darby canine kidney (MDCK) cells. Virus was propagated in MDCK cells in DMEM/F12 with ITS+ (BD Biosciences, Franklin Lakes, NJ) and trypsin, harvested at 72 h post-infection and titered by plaque assay in MDCK cells. The virus was stored in aliquots at −80 °C. No detectable endotoxin was observed in the final viral preparations, as determined by limulus amebocyte lysate assay (Cambrex, Walkersville, MD) with a lower limit of detection at 0.1EU/ml or approximately 20 pg/ml LPS. HBEC cultures were infected at a multiplicity of infection (MOI) of 1. Total cellular RNA was collected 24 hours post-infection.

RNA preparation. The total RNA from cells was extracted with Trizol using Zymo columns with modifications described below, and then assessed for quantity on a Nanodrop spectrometer and quality on an Agilent tape station. Sample N24 was further

ethanol precipitated with sodium acetate (0.1 volume of sodium acetate pH 5.2 and 2 volumes of ethanol added to the sample with incubation at -80 ^{o}C, followed by centrifugation at 4 ^{o}C and a wash with 70% v/v ethanol at 4 ^{o}C) to remove traces of Trizol reagent. 4-50 µg of total cellular RNA was polyA purified using a Lexogen polyA RNA selection kit with elution into 12 µL volume. The quality of RNA and rRNA depletion was assessed using an Agilent tape station. The RNA from step 9 of the polyA purification protocol was further purified using a Lexogen Ribocop kit in order to collect nonpolyadenylated RNA enriched in ncRNA and depleted of ribosomal RNA. The resulting RNA was then *in vitro* polyadenylated using New England Biolabs polyA polymerase from *E. coli* (product # M0276S) with incubation at 37 ^{o}C for 90 minutes and again purified using the polyA selection kit. Oxford Nanopore kit ONT RNA-SQK002 protocols including the reverse transcription step were used to prepare libraries for nanopore sequencing with 180 ng - 2µg input RNA. Oxford Nanopore R9.4 minion flow cells and the Oxford MinION platform (MinKnow 22.12.7) were used for sequencing.

Direct RNA nanopore sequencing data analysis. Oxford nanopore base calling software, Guppy (36) within Dorado version 0.3.2 (34), was used for high quality basecalling with a minimum quality score of 7 for passing reads. Minimap 2 algorithm (37) was used to align RNA sequences to the human transcriptome, GENCODE v45 (38). FLAIR v1.4 (Full Length Alternative Isoform analysis of RNA) (39) was used for analysis of alternative splicing. m6Anet software (26) was use for analysis of m6A methylation to determine sites in a sequence that are likely to be m6A methylated. m6Anet requires a minimum of 30 copies for a transcript to be analyzed. m6Anet output includes the transcript ID, nucleotide number, probability of m6A, and percent of transcripts with m6A

at that nucleotide site. Only sites with an m6A probability equal to or greater than 0.90 were included in further analysis. NanoSPA software was used to identify m6A and pseudouridine modifications(40). Differential expression was determined using DESeq2 (41).

Results and Discussion

m6A methylation, polyA tail length, and alternative splicing of mRNA transcripts in HBECs are altered by influenza exposure. In our DRS studies of influenza exposure in HBEC cells, we identified global changes in gene expression, alternative splicing, m6A methylation, and polyA tail length between influenza-exposed and mock-exposed HBECs. We detected 1,473 and 2,729 transcripts with 2 or more isoforms and 502 and 395 transcripts with m6A methylation in exposed and unexposed HBEC cells, respectively. DRS analysis of the 3 paired data sets shows high quality RNA sequencing for polyA transcripts. Table 1 shows the overview of the results of DRS analysis in polyA and nonpolyadenylated transcripts. The figures showing high accuracy basecalling at >95% are shown in Figure S1. Figures showing the accuracy of mapping reads in plots of normalized read identity versus read length are also shown in Figure S1.

Differential Transcript Expression. Table 2 lists the top 10 most significantly upregulated and downregulated transcripts related to immune response and virus entry. The many upregulated transcripts with Gene Ontology (GO) terms related to virus entry and attachment and cytokine signaling indicate that this experiment captured a snapshot of the early stages of infection. Many of the down-regulated transcripts indicate a reduction in the genes that regulate the immune response. The viral RNA transcripts were not detectable in our experiments, which is consistent with an early stage of infection

when the virus is bound to cells, but not yet entered or begun viral replication. The moderate MOI and submerged cell culture methods used in this study are conducive to studying the response of exposure to virus and virus binding to the cells, but not viral replication effects *per se*. The importance of cells responding to virus prior to active replicating infection has been highlighted in several recent single cell transcriptome profiles of bystander cells (42-44). In low MOI conditions, many cells remain uninfected but still respond to the virus infection. Interestingly, bystander cells and infected cells show different transcriptomic profiles in influenza infections (42). In addition to identifying transcripts expressed in response to exposure to influenza, our approach with nanopore DRS provides information on nucleotide modifications that is not yet technically possible in single cell studies.

m6A Methylation Patterns. Figure 2 shows the distribution of m6A methylation in different types of RNA purified from HBECs exposed or not exposed to influenza. Overall, analysis of methylation of protein coding transcripts demonstrates a preference for the GGACA motif as a target for modification with the center A being the nucleotide that is methylated. The protein coding transcripts show a wide variety of motifs that are m6A methylated, while the lncRNA and introns show a more selective usage of targeted motifs. The lncRNA motifs GGACA and AGACU are preferentially modified in HBECs overall, while enhanced modification of the AGACU motif appears to occur in response to influenza exposure. In contrast, the intron RNA show no change in motif usage with virus exposure. Shifts in motif sequence usage from AAC to GAC have been observed in Zika virus infection and were attributed to a change in substrate specificity of the methylation enzymes (45). The sequence motif usage is cell specific and idiosyncratic to

environmental conditions. The factors determining m6A site selection remain poorly understood (4). The m6A readers, writers, and erasers recognize the sequence motif DRACH or RRACH motif where D is A, G, or U; R is A or G; and H is A, C, or U. DRACH motifs occur approximately 1 in every 57 nucleotides, although only 1 in every approximately 1,000 nucleotides is m6A-methylated (4). The nucleotide accessibility, local RNA structure, and overall gene architecture contribute to sequence motif usage. In this case of influenza in HBEC cells, the factors influencing the selection of m6A motifs are distinctly different for lncRNA versus protein coding transcripts and change in response to IAV in the lncRNA transcripts.

Figure 3 shows an overlay of differentially expressed transcripts and differentially methylated transcripts between diluent-exposed and influenza-exposed HBECs. Unexpectedly, the majority of transcripts that show differential m6A do not change transcript abundance. This suggests that mechanisms to regulate transcription are independent of post-transcriptional mRNA methylation, which can regulate gene expression at the point of protein translation. Only one transcript has reduced m6A and increased transcript abundance. This transcript, *AHNAK2* (ENST00000557457.1), is part of calcium signaling pathways. Only 2 transcripts, *SEMA4B* and *HSPA5,* have reduced m6A and decreased transcript abundance. *SEMA4B* promotes tumor progression in lung cancer proliferation (46). *HSPA5* is part of the heat shock protein 70 family that has a well-studied m6A methylation at nucleotide 103 in the 5'UTR that facilitates 5'cap-independent translation using an internal ribosome entry site (47). Heat shock proteins have several roles in influenza expression and help stabilize viral proteins and viral RNA-protein interactions at every step of the viral life cycle (48). Interestingly, in our data, the

m6A and expression of *HSP5A* both are decreased. Both differential methylation and differential transcription vary during the course of infections. A comparison of differential methylation and differential transcription in *Pseudomonas aeruginosa* bacterial infections, Herpes Simplex Virus-1 (HSV-1) infection, and lipopolysaccharide treatment highlighted the dynamic changes in m6A methylation over time and in different infection contexts (12). In the case of HSV-1, there was also no observed correlation of m6A methylation and differential transcript expression in immune response (12). Thus, the methylation of RNA transcripts is a highly dynamic mechanism of gene regulation that may display wide variation over time and in different cellular and viral contexts.

m6A methylation also does not correlate with alternative splicing. Thus, m6A methylation is not likely the main mechanism of regulating the changes in alternative splicing in response to influenza. A similar lack of correlation between m6A methylation and alternative splicing was observed in a study of influenza infection in A549 cells using traditional Illumina sequencing with m6A antibody immunoprecipitation (49). The one transcript that is both m6A methylated and changes isoform expression is Calmodulin 2 (*CALM2, ENST0000272298.12)* that has 6 exons and 9 protein isoforms. *CALM2* is part of a system of 3 CALM transcripts that respond to calcium signaling, regulate cell metabolism, and are dynamically regulated by codon usage, mRNA stability, and alternative splicing in response to a wide variety of cellular stresses and disease states(50). The multiple levels of mRNA regulation for these *CALM* transcripts may enable rapid and robust responses to environmental conditions.

Two lncRNA that regulate immune response are differentially methylated in response to influenza exposure in our RNA nanopore data. Linc01578, also known as

Chaserr, is methylated at 11 sites in our data. Linc01578 regulates Chromodomain Helicase DNA Binding Protein 2 (*CHD2)* in development and directly binds *NFKB* as part of a positive feedback loop to drive carcinogenesis (51, 52). Linc00510, also known as *LEADR* and *MIR205HG*, is methylated at 6 sites in our RNA nanopore data. Linc00510 is both a pri-miRNA for miR-205 that regulates the interferon pathway and also a lncRNA that regulates *IRF1* transcription factor activity by binding upstream of the *IRF7* site through *Alu* base pairing (53, 54). The multiple m6A modifications on these regulatory lncRNA are predicted to change the shape of the lncRNA and disrupt the molecular interactions through which these lncRNA perform regulatory functions.

polyA Tail Length. There is an overall decrease in polyA tail length in response to influenza exposure (Figure 4a). Decreased polyA tail lengths are associated with reduced mRNA lifetimes in the cytoplasm and reduced translational efficiency. In our current analysis, 410 genes with GO terms related to immunity and immune regulation show a change in polyA tail length. Some notable immune regulation genes with changes in polyA tail length include *NFKB1* and *NFKB2*; *IRF2, IRF3, IRF6, IRF7*, and *IRF9*; *IL4, IL6*, and *IL32*; *STAT1, STAT2*, and *STAT6*; *TLR2*; *ISG20*; *IFITM1 and IFITM2*; *MAV*; and *OAS1*. Figure 4B shows an overlay of differentially expressed transcripts and differential polyA tail length. Interestingly, the genes with the most change in gene expression are less likely to show a change in polyA tail length. This observation suggests that there are distinct, independent mechanisms of transcriptional and post-transcriptional regulation of host response genes.

Alternative Splicing. The longread nanopore data unambiguously identifies the isoforms of transcripts that have multiple alternative splice sites. Among the top 12 differentially expressed transcripts with multiple isoforms (Table 3), the transcript for ISG12 is significantly upregulated with a 7.83 log2 fold change in response to influenza exposure. ISG12 is known to suppress viral infection through binding to nuclear receptor NR4A1 and preventing nuclear export (55). ISG12 has 8 isoforms with complex alternative splicing (Figure 5) (56). Identification of the correct isoform becomes unambiguous with the long-read sequencing in the direct RNA sequencing approach.

Transcriptional Landscape of Nonpolyadenylated RNA

In response to influenza exposure, expression of nonpolyadenylated noncoding RNA is also changed. We recovered nonpolyadenylated RNA from the polyA purification step, sequenced the transcripts with nanopore sequencing after in vitro polyadenylation, and filtered out any protein coding sequences that could be fragments of mRNA transcripts in the bioinformatic analysis. Figure 6 and SI Figure 2A show the distribution of all types of RNA after filtering out any protein-coding RNA transcripts. After the bioinformatic filtering, the distribution of types of RNA is similar in both exposed and unexposed samples. The most common nonpolyadenylated noncoding RNA include 7SL, snRNA, snoRNA, processed pseudogenes, ribozymes, lncRNA, and 7SK.

The most abundant RNA is 7SL RNA. 7SL RNA is a Pol III transcript that normally binds signal recognition particle proteins SRP9 and SRP14. However, unbound 7SL RNA is also a substrate for RIG-I (57). In RSV, VSV, and hMPV infections in A549 cells, 7SLRNA is 5mC methylated and activates the RIG-I mediated IFN response (57). 7SL

RNA can also be m6A methylated in some contexts (58), although m6A methylation in our data was not observed with high probability.

Figure 6B shows a volcano plot of the differentially expressed nonpolyadenylated noncoding RNA in response to virus exposure. Interestingly, no transcripts are induced with statistical significance, although many transcripts are down-regulated in response to influenza exposure. Table 4 lists the top ten most down regulated nonpolyadenylated noncoding RNA transcripts, which includes snoRNA of the H/ACA type (snoRA2A, snoRA33, snoRa23, snoRA74D), one type of 7SL RNA (rn7SL5P), small nuclear RNA RNU4ATAC, small Cajal body-specific RNA 7 (scaRNA7, a subtype of snoRNA), and 5.8S rRNA. Dysregulation of snoRNA has been previously reported for PR8 influenza infection in A549 cells(58), but no clear mechanism was proposed. In addition to guiding pseudouridylation, snoRNA also are used by influenza viruses in cap snatching (59-61). Furthermore, snoRNA binding sites correlate with hotspots for recombination in the hemagglutinin genomic RNA (62). Thus, snoRNA have multiple functions in addition to pseudouridylation of ribosomal RNA that play a role in the virus-host interactions in influenza.

Pseudouridylation. Consistent with the downregulation of H/ACA type snoRNA, there is a decrease in pseudouridylation in some nonpolyadenylated ncRNA. Pseudouridylation was identified using the NanoSPA software that detects both m6A and pseudouridylation (40). The program accurately identified well-known pseudouridylation sites on 5.8S rRNA at nucleotides 69 and 55 (63) with 95% and 85% probabilities, respectively. Thus, the 90% probability cutoff that we used is a conservative identification of pseudouridylation sites. In addition to several ribosomal RNA pseudogenes,2 lncRNA

were differentially pseudouridylated in response to influenza (SI Table 1). Two lncRNA, linc00273 and novel lncRNA ENST 00000625598.1, are highly pseudouridylated in unexposed cells but not in exposed cells. Linc00273 has 19 high probability pseudouridylated sites in unexposed cells, but none in exposed cells. Linc00273 is transcriptionally induced by STAT3 and plays a role in M2 macrophage activation (64). Linc00273 also acts as molecular sponge for miR-200a-3p and promotes lung cancer metastasis(65). The expression of linc00273 does not change significantly, only its pseudouridylation. This lincRNA is not polyadenylated; and thus this ncRNA may not have been previously identified as having a role in response to influenza infection. ENST00000625598.1 is a 923-nucletoide novel antisense lncNRA whose function is yet unidentified. In diluent-exposed cells, the transcript has 16 high probability pseudouridylation sites, while in IAV-exposed cells the lncRNA has no predicted psuedouridylation sites. Further research may reveal the role of these lncRNA and their pseudouridylation in influenza.

m6A methylation. Only one nonpolyadenylated lncRNA was predicted to be differently m6A methylated using nanoSPA. Transcript ENST00000629969.1 is a 923 nucleotide antisense lncRNA with no known function. Nucleotide 492 of this transcript is identified as m6A methylated, but not in response to influenza. Interestingly, this modification is predicted to destabilize the RNA secondary structure. Figure 7 shows the predicted centroid RNA secondary structure for the unmodified and modified sequences. The m6A modification reduced the probability of the helix in which it forms a base pair and also the probabilities of base pairing in the surrounding helices. One helix adjacent to a large junction is no longer predicted to form at all. This example highlights the

possible structural mechanisms of m6A methylation that can change RNA structure and interactions with small molecule drugs and proteins.

Conclusion. This study profiles the epitranscriptomic changes in host bronchial epithelial cells in the early stages of influenza virus infection. The study includes mRNA transcripts, polyadenylated noncoding RNA, and nonpolyadenylated noncoding RNA. The epitranscriptomic modification of noncoding RNA extends the mechanistic repertoire of noncoding RNA gene regulation to include changing RNA interactions at the post-transcription stage in response to environmental cues, stresses, and infections. There is a decrease in H/ACA type snoRNA and a decrease in pseudouridylation of several noncoding RNA. The m6A methylation patterns are distinctly different for coding and noncoding RNA. Unexpectedly, m6A methylation did not correlate with alternative splicing, polyA tail length, or differential expression. Alternatively, the m6A and pseudo modifications may change RNA cellular stability, RNA folding, or RNA interactions with proteins, small molecules, and other RNA. The potential for m6A to alter RNA secondary structure is demonstrated for a novel lncRNA. The use of direct RNA nanopore sequencing highlights the ability to identify in one experiment the differential expression, modifications, polyA tail length, and unambiguous splicing isoform in the human transcriptome and directly test correlations of modifications and the mechanisms with which modification fine tune gene expression. The ability to identify multiple modifications on a long read of an individual RNA molecule surpasses other techniques based on cleaving or fragmenting the nucleic acids for short read sequencing. For example, the linc00273 has multiple pseudouridylation sites, and this example provides a foundation

for further testing the functional role of this extensive pseudouridylation. As a single molecule experiment, nanopore direct RNA sequencing has the potential to reveal individual variations that bulk sequencing would obscure. This study presents an epitranscriptome profile that provides a foundation for future discovery of the mechanisms through which noncoding RNA and RNA modifications fine tune the host response to influenza infections.

Acknowledgement

Research reported in this publication was supported by the National Institute of General Medical Sciences of the National Institutes of Health under Award Number P20GM103648 and P30GM149368. The content is solely the responsibility of the authors and does not necessarily represent the official views of the National Institutes of Health. Research reported in this publication was supported by the Merit Review Program of the Department of Veterans Affairs, grant number I01 BX005023 (JPM); Clinical Innovator Award from the Flight Attendant Medical Research Institute # 113052 (JPM); resources and assistance from the Civil Aerospace Medical Institute, Federal Aviation Administration (JPM); a Seed Grant Award from the Presbyterian Health Foundation (JPM and SJS), the Dodge Family College of Arts and Sciences Collaborative Fellowships Award at the University of Oklahoma (SJS); and an MCI supplement to NSF TRTech Award #2023310 (SJS). The funders had no role in study design, data collection and interpretation, or the decision to submit the work for publication. We thank the Consolidated Core Lab at the University of Oklahoma for the use of the facility that provided nanopore sequencing resources and equipment.

Table 1. Direct RNA Sequencing Analysis of Transcripts in Human Bronchial Epithelial Cells Exposed to IAV

sample	reads mapped	reads with m6A	reads > 1 alternative splicing event	Differentially expressed reads	reads with differential polyA tail
polyA transcripts					
Donor 1 uninfected	1448955	4129	10626	11527	3037
Donor 1 Infected	1548820	6657	9383		
Donor 2 uninfected	669296	1695	5797		
Donor 2 Infected	442279	4205	5434		
Donor 3 uninfected	200368	236	2389		
Donor 3 Infected	282294	196	2711		
Nonpolyadenylated transcripts					
Donor 1 uninfected	8909	0	0	44	Not applicable
Donor 1 Infected	748	0	0		
Donor 2 uninfected	112016	1	0		
Donor 2 Infected	2224	0	0		

Table 1 Legend: The p-value was adjusted as p-adjust by the method of Benjamin Hochberg (66). The cut off for p-adjust is 0.05. The cutoff of for log2 fold change in differentially expressed genes is 1.2. The lowest probability cutoff for m6A methylation in m6Anet is 0.90.

Table 2A: Transcripts Up-Regulated in Response to IAV Exposure and Related to Immune Response and Virus Entry

ID	Common name	log2FoldChange	pvalue	padj	GO Term Description
ENST00000359228.4	LYPD2-201	29.59568873	1.93e-17	1.19e-14	negative regulation of interleukin-6-mediated signaling pathway negative regulation of interleukin-4-mediated signaling pathway
ENST00000597959.1	Novel protein	28.32018644	9.15e-17	2.98e-14	negative regulation of viral entry into host cell
ENST00000319720.11	KLK11-201	28.30002807	4.60e-16	7.77e-14	response to interferon-beta, response to interferon-gamma, response to interferon-alpha, type I interferon signaling pathway
ENST00000291009.4	BRST-2	27.90139034	4.27e-16	7.47e-15	innate immune response, defense response to virus, cellular response to virus
ENST00000226796.7	NOLA1	27.40524808	1.90e-15	2.06e-13	viral entry into host cell, T cell antigen processing and presentation, leukocyte cell-cell adhesion, cell adhesion mediated by integrin
ENST00000455878.2	Proteasome 26S ATPase	27.38923998	6.21e-15	5.14e-13	virus receptor activity, negative regulation of extrinsic apoptotic signaling pathway via death domain receptors, heterophilic cell-cell adhesion via plasma membrane cell adhesion molecules, regulation of leukocyte mediated cytotoxicity, T cell activation via T cell receptor contact with antigen bound to MHC molecule on antigen presenting cell
ENST00000574838.1	TXNDC17-208	27.38232723	1.90e-15	2.06e-13	receptor-mediated virion attachment to host cell
ENST00000356053.7	HNRPF	27.12578158	5.94e-14	3.07e-12	cytokine activity, immune response, cytokine-mediated signaling pathway, signaling receptor binding
ENST00000506797.5	MGST-11	26.75154118	8.98e-14	4.34e-12	viral entry into host cell
ENST00000238379.9	HDHD3-201	26.72771535	1.07e-13	5.04e-12	virus receptor activity

Table 2B: Transcripts Down-Regulated in Response to IAV Exposure and Related to Immune Response and Virus Entry

ID	Common name	log2FoldChange	pvalue	padj	GO Term Description
ENST00000374515.9	TRX80	-29.27946318	3.01e-14	1.45e-14	viral entry into host cell
ENST00000556102.6	CDKN3	-28.76614587	1.33e-17	9.45e-15	positive regulation of interleukin-1 production, macrophage chemotaxis
ENST00000551217.1	RPLP0	-28.76504359	9.34e-17	3.00e-14	positive regulation of cytokine production
ENST00000594552.5	Calpain 12	-28.76385654	3.46e-17	1.60e-14	negative regulation of inflammatory response
ENST00000576984.3	CD147	-28.75394799	4.15e-16	7.31e-14	immune response, antigen processing and presentation
ENST00000679733.1	TUBA1A	-28.43354291	9.10e-16	1.22e-13	toll-like receptor 9 signaling pathway, toll-like receptor 4 signaling pathway
ENST00000465783.6	MKNK1	-28.41311942	5.84e-17	2.29e-14	toll-like receptor 2 signaling pathway, positive regulation of type I interferon production
ENST00000591341.1	NDUFA11	-28.39596418	1.10e-16	3.39e-14	NF-kappaB-inducing kinase activity
ENST00000395284.8	CDK1-203	-28.37737858	4.02e-16	7.12e-14	innate immune response, toll-like receptor signaling pathway, type I interferon signaling pathway, response to interleukin-1, negative regulation of NF-kappaB transcription factor activity, activation of NF-kappaB-inducing kinase activity
ENST00000394149.8	CSF3-204	-28.04353973	1.03e-15	1.34e-13	negative regulation of interferon-gamma production, negative regulation of interleukin-17 production

Table 2: The transcript ID follow the Ensembl database nomenclature (67). The log2 fold change and the adjusted p-value was determined using DESeq (41) and the method of Benjamin Hochberg (66).

Table 3: Alternatively Spliced Transcripts Related to Immune Response in Response to IAV Exposure

ID	Common name	log2FoldChange	pvalue	padj	GO Term Description
ENST00000621160.5	ISG12	7.834827	0.000109007	0.026674	immune system process, defense response to virus, type I interferon signaling pathway, innate immune response
ENST00000307407.8	IL8	-7.54897	0.000391257	0.059838	CXC motif chemokine ligand 8
ENST00000393820.2	Nucleophosmin 1	7.999073	0.000779847	0.082042	NF-kappaB binding, positive regulation of NF-kappaB transcription factor activity
ENST00000495461.6	SeleneOK	7.463205	0.000966527	0.090965	positive regulation of defense response to virus by host, macrophage derivd foam cell differentiation, positive regulation of interleukin-6 production, positive regulation of tumor necrosis factor production, T cell proliferation, T cell migration, positive regulation of neutrophil migration, neutrophil migration, positive regulation of T cell migration
ENST00000476133.6	S100 calcium binding protein A13	-7.73135	0.001269425	0.098032	positive regulation of cytokine production, positive regulation of interleukin-1 alpha production, positive regulation of I-kappaB kinase/NF-kappaB signaling
ENST00000525643.7	IL-32	-7.33409	0.0033791	0.168748	cytokine activity, defense response, immune response
ENST00000234875.9	L22	-11.2251	0.004064586	0.181123	alpha-beta T cell differentiation
ENST00000300289.10	PDIA3	-7.10807	0.004556396	0.186878	cellular response to interleukin-7
ENST00000280357.12	IL18-201	-7.09312	0.004878905	0.195541	Interleukin 18
ENST00000367351.4	RAET1H	-6.76689	0.009165006	0.258238	positive regulation of T cell mediated cytotoxicity, immune system processes, antigen processing and presentation of endogenous peptide antigen via MHC class Ib, immune response, natural killer cell activation

Table 3: The transcript ID follow the Ensembl database nomenclature (67). The log2 fold change and the adjusted p-value was determined using DESeq (41) and the method of Benjamin Hochberg (66).

Table 4. Most Down-Regulated Nonpolyadenylated Noncoding RNA in Response to IAV Exposure

Transcript ID	Common Name	Log2FC	Adj. P-value
ENST00000383885.1	SNORA2A	-12.7089	0.000144
ENST00000581458.2	RN7SL5P	-12.5555	0.000144
ENST00000363664.1	SNORA33	-12.4268	0.000142
ENST00000580972.1	RNU4ATAC	-12.3731	0.000142
ENST00000458797.1	SCARNA7	-12.3306	0.000142
ENST00000365128.1	SNORA23	-12.3157	0.000142
ENST00000612463.1	RNA5-8SN2	-12.1294	0.000142
ENST00000619471.1	RNA5-8SN1	-11.9426	0.000145
ENST00000610460.1	5_8S_rRNA	-11.8317	0.000142
ENST00000516404.1	SNORA74D	-11.4238	0.000172

Table 4: The transcript ID follow the Ensembl database nomenclature (67). The log2 fold change and the adjusted p-value was determined using DESeq (41) and the method of Benjamin Hochberg (66).

Figure 1: N6-methyl-adenosine (m6A) and Pseudouridine (Ψ)

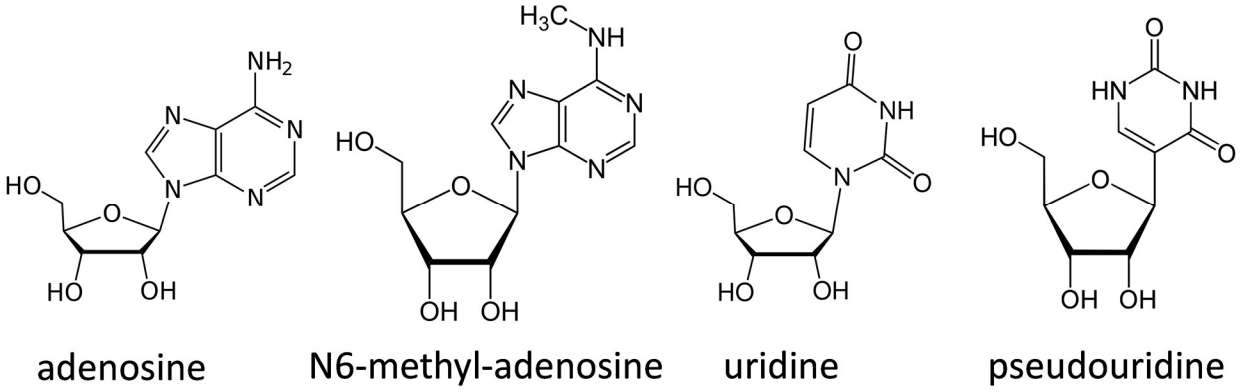

Figure 1: The chemical structure of adenosine, methyl-6-adenosine, uridine, and pseudouridine. N6-methyl-adenosine (m6A) can be directly detected using m6A net analysis of nanopore direct RNA sequence (DRS) data (26). NanoSPA identifies both m6A and pseudouridine (Ψ) in DRS data (68). In response to exposure to influenza A virus (IAV), both m6A and Ψ change dynamically.

Figure 2: Methylation Motifs in Different Types of RNA after Exposure to IAV

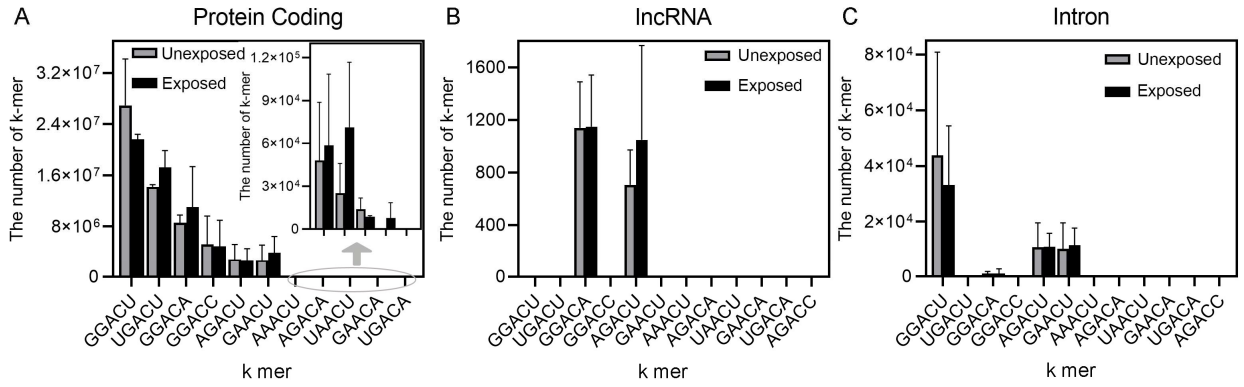

Figure 2. For each type of polyadenylated RNA, a histogram shows the number of each type of sequence motif that contain the m6A at the center of the motif. GGACU was the most common site of m6A in all types of RNA. The gray bars represent uninfected control samples, and the black bars represent the infected samples.

Figure 3: **Changes in m6A Methylation are Rare in Transcripts with the Largest Change in Expression in Response to IAV Exposure**

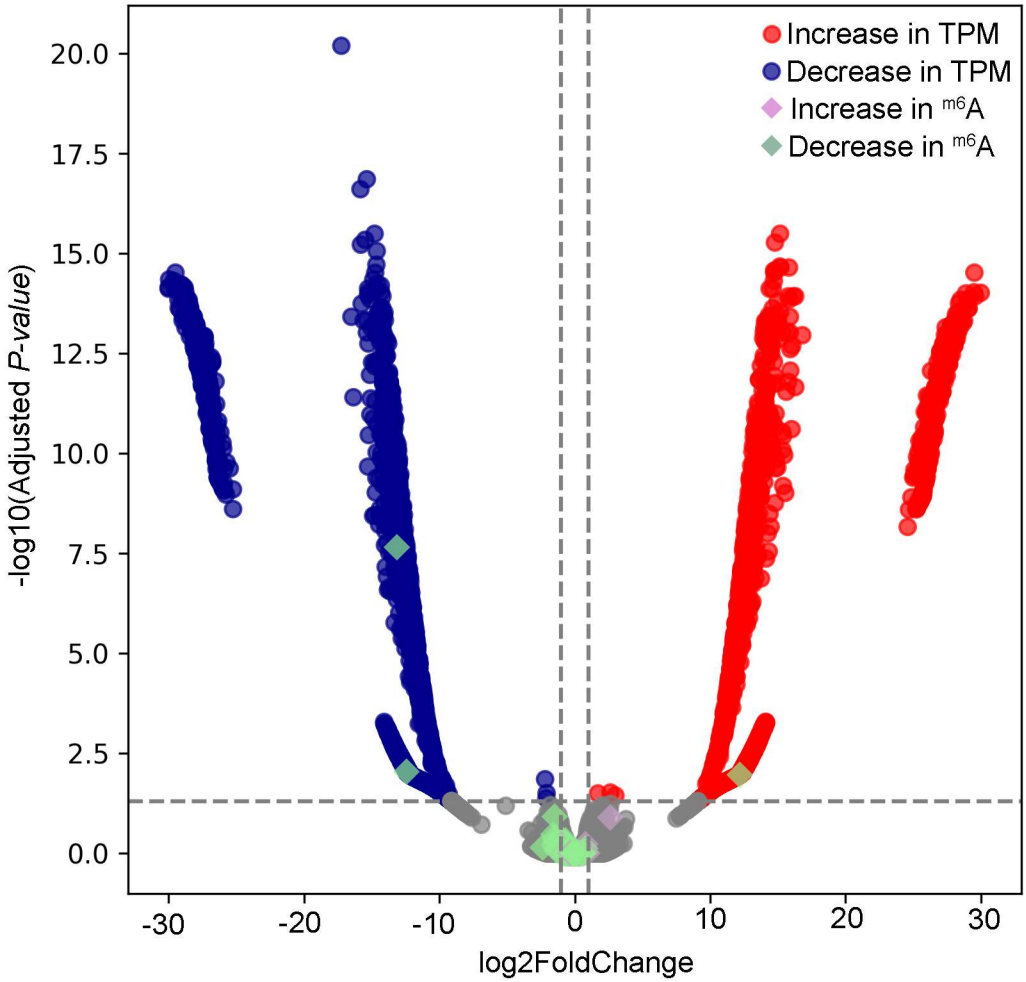

Figure 3. Volcano plot shows the log2 fold change versus for log 10 adjusted p-value for differential gene expression in uninfected versus infected HBEC cells. The red circles are overexpressed genes. The blue circles are underexpressed genes. The green diamonds indicate genes that are also m6A methylated and decrease in expression level. The purple diamonds indicate genes that are m6A methylated and increase in expression level.

Figure 4: Global Changes in polyA Tail Length with Influenza Exposure

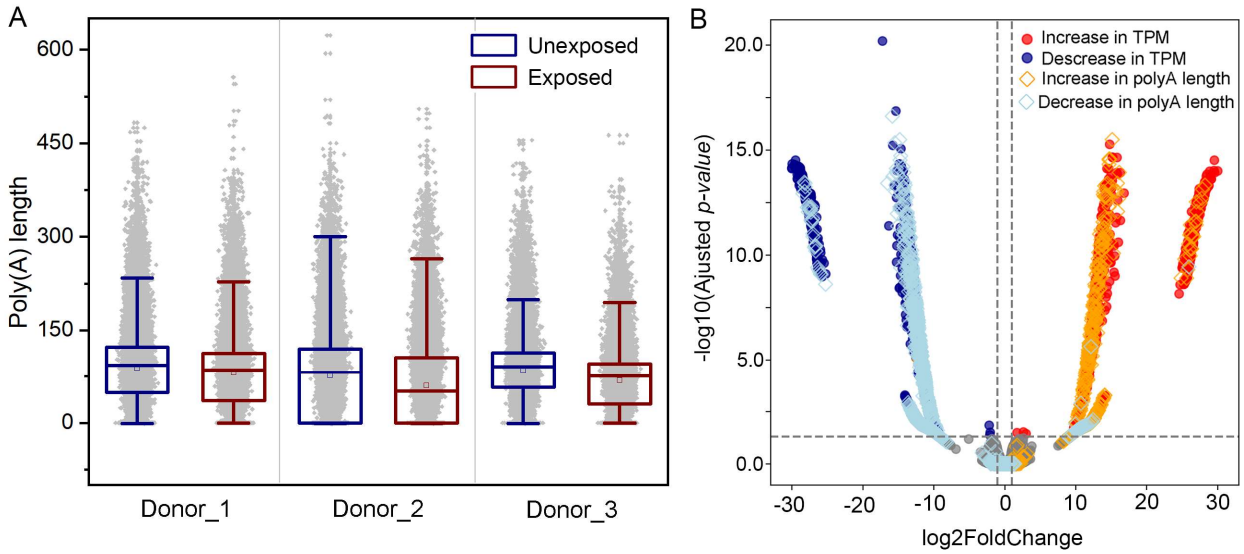

Figure 4: A. Distribution of polyA tail length in each data set. B. Volcano plot shows the log2 fold change versus for log 10 adjusted p-value for differential gene expression in uninfected versus infected HBEC cells. The red circles are overexpressed genes. The blue circles are underexpressed genes. The orange and light blue diamonds indicate transcripts that also change polyA tail length.

Figure 5: Alternative Splicing of ISG12 (IFI27-213) in Response to IAV Exposure

Figure 5: Transcript ISG12. Interferon Stimulated Gene 12 (ISG12) is also known as IFI27-213 (ENST00000621160.5). Interferon α Inducible Protein 27 is one of 8 isoforms. The DNA sequence spans 5.96 kb. The gene has 4 splice sites. 4 introns, 5 exons, and 4 coding exons (filled boxes). The primary transcript is the longest and has 652 nucleotides that code for a protein with 122 amino acids(56). The filled boxes indicate the coding exons expressed as a protein in response to IAV, thus highlighting the specific isoform observed to increase expression in our data. Such complex alternative splicing is difficult to identify in short-read sequencing with data from reads 100-200 bp in length. In short-read sequencing, few reads overlap the splice site junction and can be mapped unambiguously to a specific isoform.

Figure 6. Nonpolyadenylated Noncoding RNA Transcriptome Profiles in Response to IAV Exposure

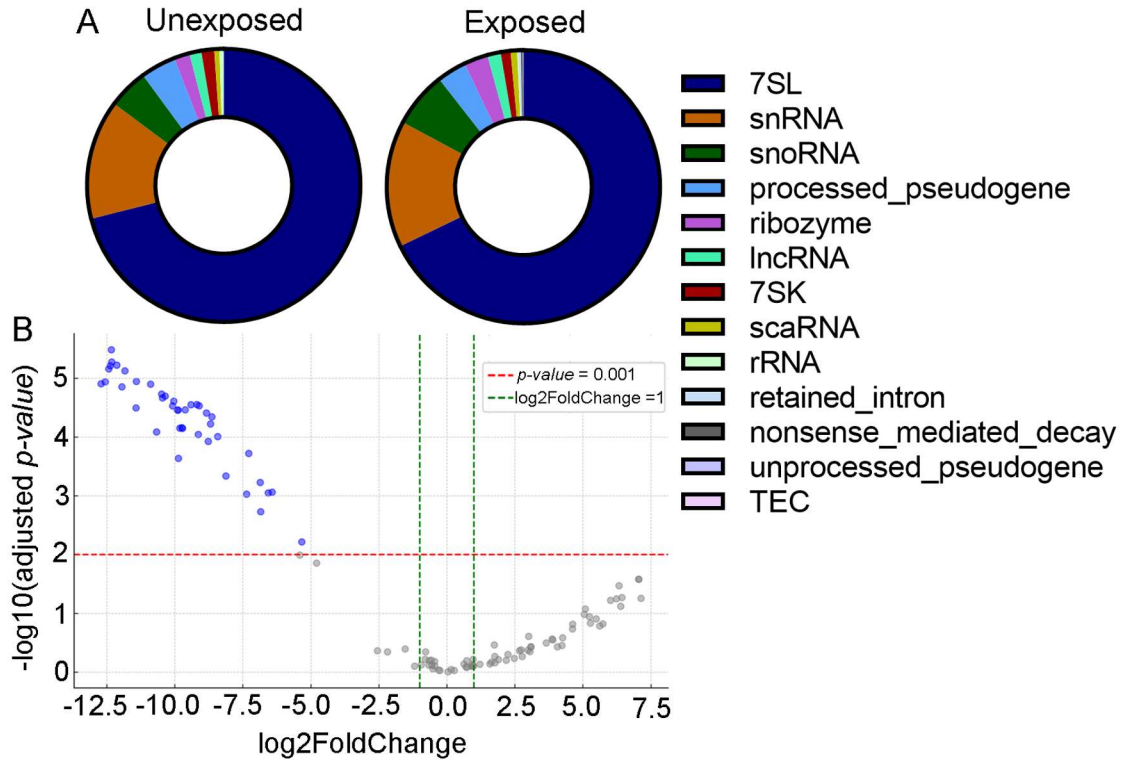

Figure 6. A. Distribution of types of nonpolyadenylated noncoding RNA in uninfected and PR8-infected HBEC cells by TPM. The total number of unique transcripts is 114. Key: 7SL dark blue; small nuclear RNA (snRNA) orange; small nucleolar RNA (snoRNA) dark green; processed pseudogenes sky blue; ribozymes purple; long noncoding RNA (lncRNA) lime green; 7SK RNA red; small Cajal body associate RNA (scaRNA) gold; ribosomal RNA (rRNA) light green; retained intron light gray; nonsense mediated decay red; unprocessed pseudogenes dark gray; unprocessed pseudogenes, light purple; to be experimentally confirmed (TEC), pink. B. The log2 fold change and the adjusted p-value was determined using DESeq (41). The dots in blue are statistically significant with a p-adjusted value cutoff of 0.05 using the Benjamin Hochberg method (66).

Figure 7. Predicted Structural Effects of m6A in a lncRNA that Responds to IAV Exposure

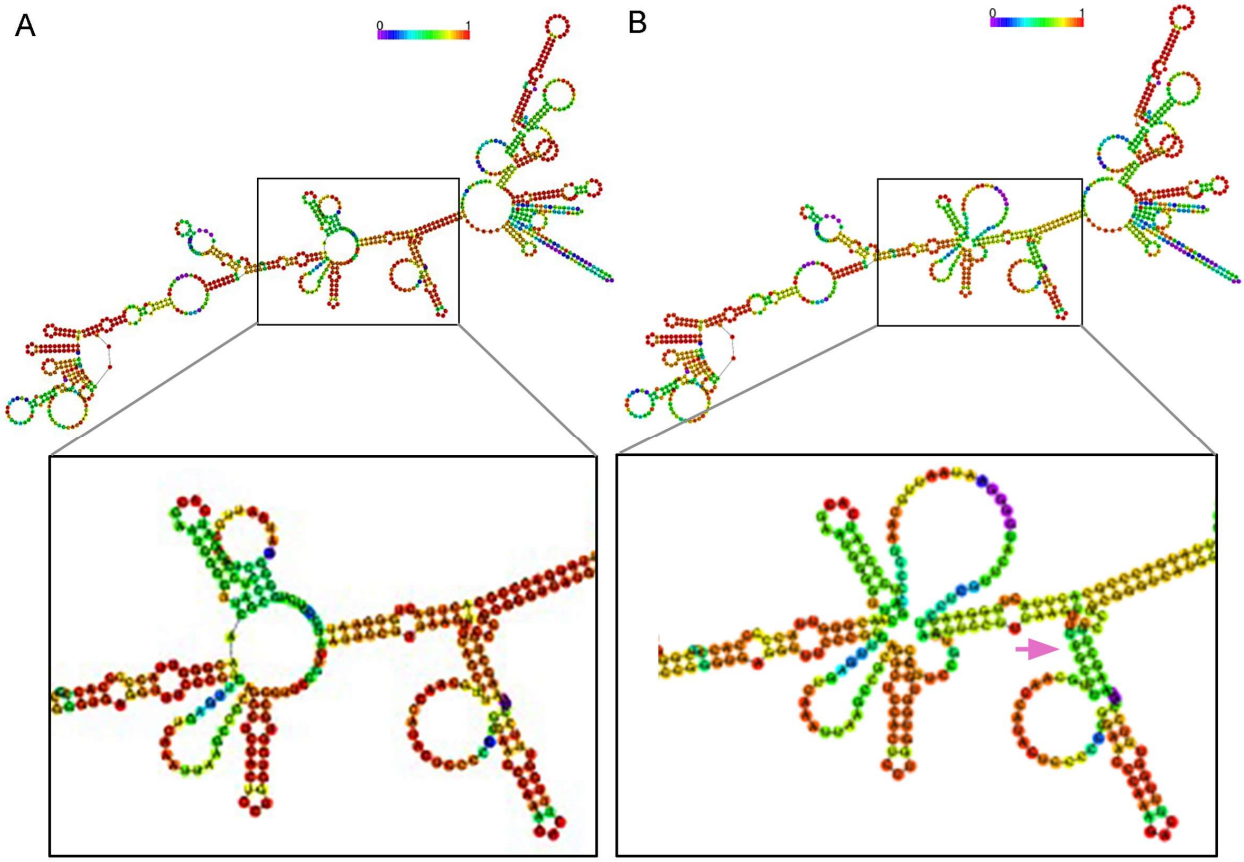

Figure 7. Predicted centroid secondary structures for ENST00000629969.1 without (A) and with (B) m6A at nucleotide 492. The color of the nucleotide indicates the probability of the nucleotide being in a base pair or unpaired with red being a probability of 1 and purple being a probability of zero. Structures were generated using Vienna rnafold in May 8,2024 (69). The pink arrow in B indicates the location of the m6A modification.

SI Table 1: Nonpolyadenylated Noncoding RNA with Changes in PSeudouridylation Induced by IAV Exposure

Transcript	Common name	Ψ sites, uninfected	Ψ sites, infected
ENST00000539813.1	Linc00273	323, 350, 430, 553, 583, 674, 700, 716, 758, 773, 833, 838, 851, 876, 903, 917, 969, 1033, 1042	none
ENST00000625598.1	Novel lncRNA	45, 46, 61, 68, 291, 292, 423, 478, 484, 494, 593, 613, 692, 871	none
ENST00000445125.2	18 S ribosomal pseudogene Y chromosome	35, 99, 109, 461, 517, 568, 572, 590, 648, 707, 957, 1108, 1226, 1236, 1339, 1566	none
ENST00000445125.2	18 S ribosomal pseudogene Y chromosome	none	1782

SI Table 2: Pseudouridylation sites were identified using nanoSPA (40) and a cutoff of 90% probability. Only sites consistently identified in both donors are included.

SI Figure 1: RNA Quality and Basecalling Accuracy

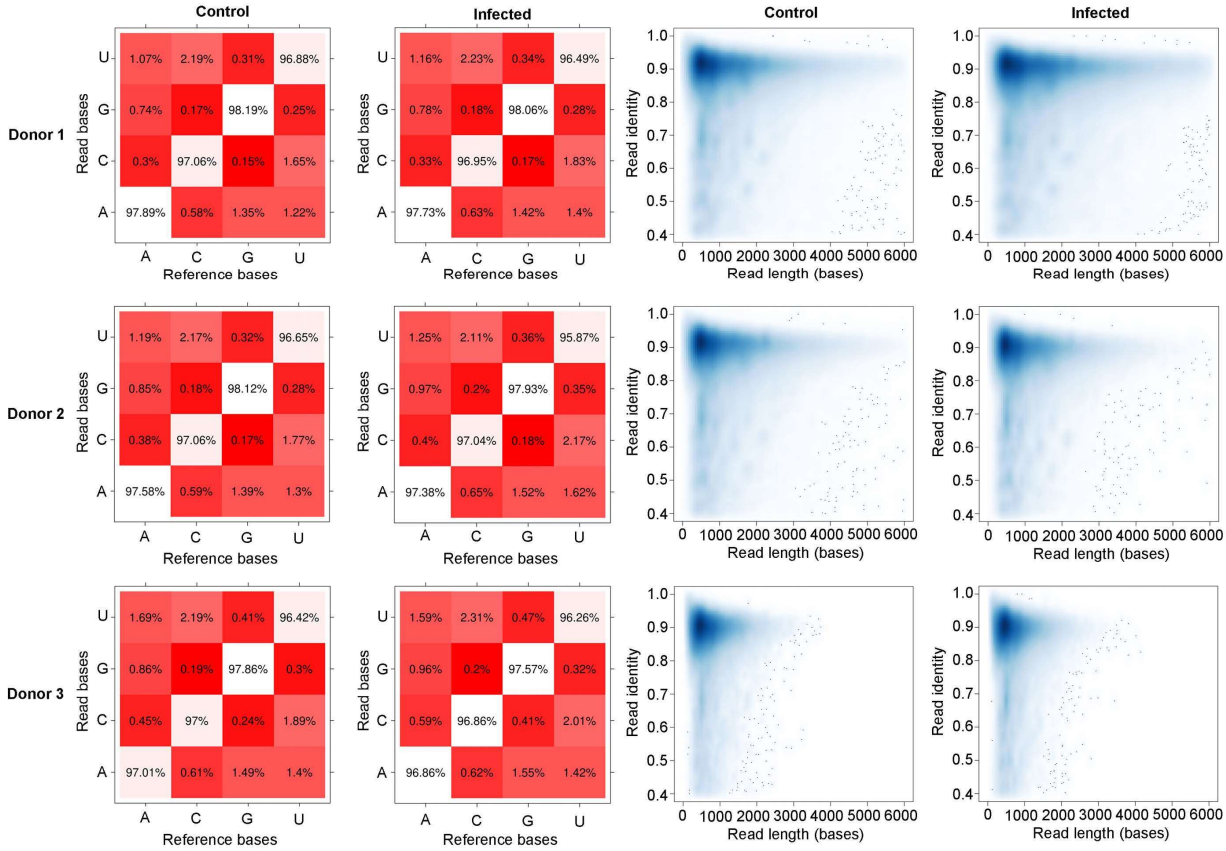

SI Figure 1: Base calling accuracy plots and normalized read identity versus length plots were calculated following the analysis used by Workman et al.(8).

SI Figure 2. Noncoding RNA Profiles Induced by IAV Exposure for Each Donor

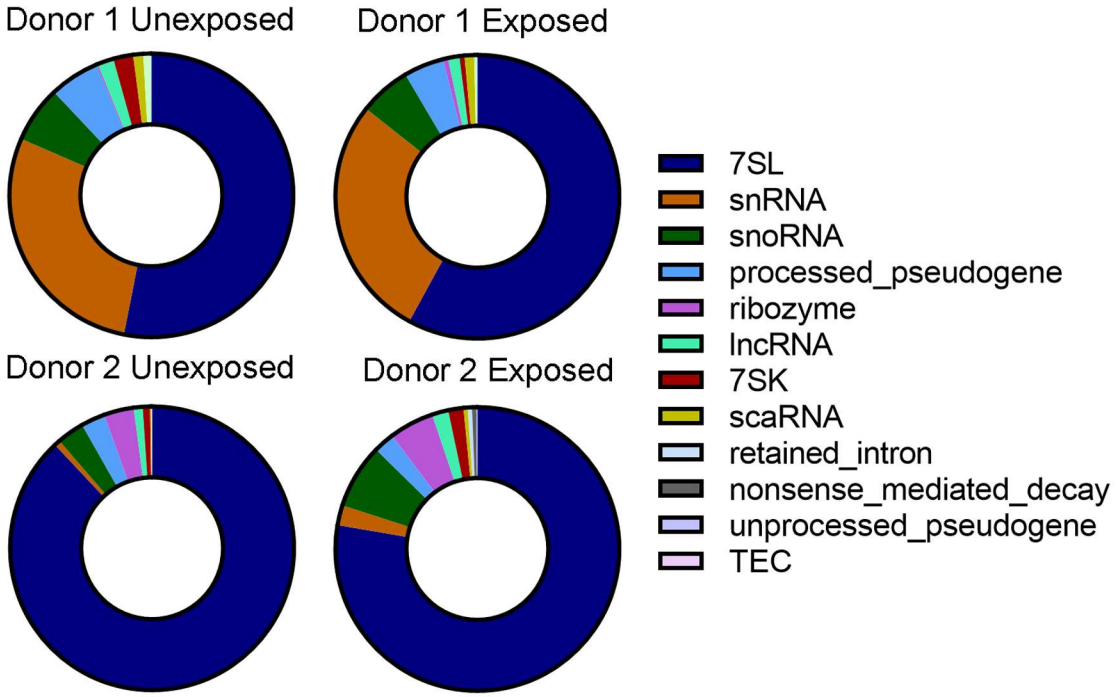

SI Figure 2. Distribution of types of nonpolyadenylated noncoding RNA in uninfected and IAV-exposed HBEC cells for each donor data set by TPM. Key: 7SL dark blue; small nuclear RNA (snRNA) orange; small nucleolar RNA (snoRNA) dark green; processed pseudogenes sky blue; ribozymes purple; long noncoding RNA (lncRNA) lime green; 7SK RNA red; small Cajal body associate RNA (scaRNA) gold; ribosomal RNA (rRNA) light green; retained intron light gray; nonsense mediated decay red; unprocessed pseudogenes dark gray; unprocessed pseudogenes, light purple; to be experimentally confirmed (TEC), pink.

References

1. Centers for Disease Control 2023. Disease Burden of Flu. https://www.cdc.gov/flu/about/burden/index.html. Accessed September 4, 2023.
2. Arribas-Hernández L, Rennie S, Köster T, Porcelli C, Lewinski M, Staiger D, Andersson R, Brodersen P. 2021. Principles of mRNA targeting via the Arabidopsis m6A-binding protein ECT2. eLife 10:e72375.
3. Macveigh-Fierro D, Cicerchia A, Cadorette A, Sharma V, Muller M. 2022. The m(6)A reader YTHDC2 is essential for escape from KSHV SOX-induced RNA decay. Proc Natl Acad Sci U S A 119.
4. Murakami S, Jaffrey SR. 2022. Hidden codes in mRNA: Control of gene expression by m6A. Molecular Cell 82:2236-2251.
5. Li N, Hui H, Bray B, Gonzalez GM, Zeller M, Anderson KG, Knight R, Smith D, Wang Y, Carlin AF, Rana TM. 2021. METTL3 regulates viral m6A RNA modification and host cell innate immune responses during SARS-CoV-2 infection. Cell Reports 35:109091.
6. Xiao W, Adhikari S, Dahal U, Chen YS, Hao YJ, Sun BF, Sun HY, Li A, Ping XL, Lai WY, Wang X, Ma HL, Huang CM, Yang Y, Huang N, Jiang GB, Wang HL, Zhou Q, Wang XJ, Zhao YL, Yang YG. 2016. Nuclear m(6)A Reader YTHDC1 Regulates mRNA Splicing. Mol Cell 61:507-519.
7. Lorenz DA, Sathe S, Einstein JM, Yeo GW. 2020. Direct RNA sequencing enables m6A detection in endogenous transcript isoforms at base-specific resolution. RNA 26:19-28.

8. Workman RE, Tang AD, Tang PS, Jain M, Tyson JR, Razaghi R, Zuzarte PC, Gilpatrick T, Payne A, Quick J, Sadowski N, Holmes N, de Jesus JG, Jones KL, Soulette CM, Snutch TP, Loman N, Paten B, Loose M, Simpson JT, Olsen HE, Brooks AN, Akeson M, Timp W. 2019. Nanopore native RNA sequencing of a human poly(A) transcriptome. Nature Methods 16:1297-1305.

9. Tsai K, Cullen BR. 2020. Epigenetic and epitranscriptomic regulation of viral replication. Nature reviews Microbiology 18:559-570.

10. Wu W, Zhang W, Tian L, Brown BR, Walters MS, Metcalf JP. 2020. IRF7 Is Required for the Second Phase Interferon Induction during Influenza Virus Infection in Human Lung Epithelia. Viruses 12:377.

11. Winkler R, Gillis E, Lasman L, Safra M, Geula S, Soyris C, Nachshon A, Tai-Schmiedel J, Friedman N, Le-Trilling VTK, Trilling M, Mandelboim M, Hanna JH, Schwartz S, Stern-Ginossar N. 2019. m6A modification controls the innate immune response to infection by targeting type I interferons. Nature immunology 20:173-182.

12. Feng J, Zhang T, Sorel O, Meng W, Zhang X, Lai Z, Yuan W, Chen Y, Huang Y, Gao S-J. 2022. Global profiling reveals common and distinct N6-methyladenosine (m6A) regulation of innate immune responses during bacterial and viral infections. Cell Death & Disease 13:234.

13. Price AM, Hayer KE, McIntyre ABR, Gokhale NS, Abebe JS, Della Fera AN, Mason CE, Horner SM, Wilson AC, Depledge DP, Weitzman MD. 2020. Direct RNA sequencing reveals m6A modifications on adenovirus RNA are necessary for efficient splicing. Nature Communications 11:6016.

14. Xue M, Zhang Y, Wang H, Kairis EL, Lu M, Ahmad S, Attia Z, Harder O, Zhang Z, Wei J, Chen P, Gao Y, Peeples ME, Sharma A, Boyaka P, He C, Hur S, Niewiesk S, Li J. 2021. Viral RNA N6-methyladenosine modification modulates both innate and adaptive immune responses of human respiratory syncytial virus. PLoS Pathog 17:e1010142.

15. Liu Y, Liu Z, Tang H, Shen Y, Gong Z, Xie N, Zhang X, Wang W, Kong W, Zhou Y, Fu Y. 2019. The N6-methyladenosine (m6A)-forming enzyme METTL3 facilitates M1 macrophage polarization through the methylation of STAT1 mRNA. American Journal of Physiology-Cell Physiology 317:C762-C775.

16. Han X, Liu L, Huang S, Xiao W, Gao Y, Zhou W, Zhang C, Zheng H, Yang L, Xie X, Liang Q, Tu Z, Yu H, Fu J, Wang L, Zhang X, Qian L, Zhou Y. 2023. RNA m6A methylation modulates airway inflammation in allergic asthma via PTX3-dependent macrophage homeostasis. Nature Communications 14:7328.

17. Kupsco A, Gonzalez G, Baker BH, Knox JM, Zheng Y, Wang S, Chang D, Schwartz J, Hou L, Wang Y, Baccarelli AA. 2020. Associations of smoking and air pollution with peripheral blood RNA N(6)-methyladenosine in the Beijing truck driver air pollution study. Environ Int 144:106021.

18. McIntyre W, Netzband R, Bonenfant G, Biegel JM, Miller C, Fuchs G, Henderson E, Arra M, Canki M, Fabris D, Pager CT. 2018. Positive-sense RNA viruses reveal the complexity and dynamics of the cellular and viral epitranscriptomes during infection. Nucleic Acids Res 46:5776-5791.

19. McIntyre W, Netzband R, Bonenfant G, Biegel JM, Miller C, Fuchs G, Henderson E, Arra M, Canki M, Fabris D, Pager CT. 2018. Positive-sense RNA viruses

reveal the complexity and dynamics of the cellular and viral epitranscriptomes during infection. Nucleic Acids Research 46:5776-5791.

20. Netzband R, Pager CT. 2019. Epitranscriptomic marks: Emerging modulators of RNA virus gene expression. WIREs RNA n/a:e1576.

21. Courtney DG, Kennedy EM, Dumm RE, Bogerd HP, Tsai K, Heaton NS, Cullen BR. 2017. Epitranscriptomic Enhancement of Influenza A Virus Gene Expression and Replication. Cell host & microbe 22:377-386.e5.

22. Mirza AH, Bram Y, Schwartz RE, Jaffrey SR. 2024. SCARPET: site-specific quantification of methylated and nonmethylated adenosines reveals m(6)A stoichiometry. Rna 30:308-324.

23. Liu N, Parisien M, Dai Q, Zheng G, He C, Pan T. 2013. Probing N6-methyladenosine RNA modification status at single nucleotide resolution in mRNA and long noncoding RNA. Rna 19:1848-56.

24. Liu H, Begik O, Lucas MC, Ramirez JM, Mason CE, Wiener D, Schwartz S, Mattick JS, Smith MA, Novoa EM. 2019. Accurate detection of m6A RNA modifications in native RNA sequences. Nature Communications 10:4079.

25. Cozzuto L, Delgado-Tejedor A, Hermoso Pulido T, Novoa EM, Ponomarenko J. 2023. Nanopore Direct RNA Sequencing Data Processing and Analysis Using MasterOfPores. Methods Mol Biol 2624:185-205.

26. Hendra C, Pratanwanich PN, Wan YK, Goh WSS, Thiery A, Göke J. 2022. Detection of m6A from direct RNA sequencing using a multiple instance learning framework. Nature Methods 19:1590-1598.

27. Zhong Z-D, Xie Y-Y, Chen H-X, Lan Y-L, Liu X-H, Ji J-Y, Wu F, Jin L, Chen J, Mak DW, Zhang Z, Luo G-Z. 2023. Systematic comparison of tools used for m6A mapping from nanopore direct RNA sequencing. Nature Communications 14:1906.

28. Artic Network 2019. ARTIC Network: Real-time Molecular Epidemiology for Outbreak Response. DOI: https://artic.network/ Accessed February 10, 2024.

29. Oxford Nanopore Technology. 2019. ARTIC Network. DOI: https://nanoporetech.com/about-us/news/artic-network-provides-protocol-rapid-accurate-sequencing-novel-coronavirus-ncov-2019 Accessed February 10, 2024.

30. Quick J, Grubaugh ND, Pullan ST, Claro IM, Smith AD, Gangavarapu K, Oliveira G, Robles-Sikisaka R, Rogers TF, Beutler NA, Burton DR, Lewis-Ximenez LL, de Jesus JG, Giovanetti M, Hill SC, Black A, Bedford T, Carroll MW, Nunes M, Alcantara LC, Sabino EC, Baylis SA, Faria NR, Loose M, Simpson JT, Pybus OG, Andersen KG, Loman NJ. 2017. Multiplex PCR method for MinION and Illumina sequencing of Zika and other virus genomes directly from clinical samples. Nature Protocols 12:1261-1276.

31. Artic Network A. 2017. ARTIC tools. DOI: https://artic-tools.readthedocs.io/en/latest/ Accessed FEbruary 10, 2024.

32. Narayan P, Ayers DF, Rottman FM, Maroney PA, Nilsen TW. 1987. Unequal distribution of N6-methyladenosine in influenza virus mRNAs. Mol Cell Biol 7:1572-5.

33. Keller MW, Rambo-Martin BL, Wilson MM, Ridenour CA, Shepard SS, Stark TJ, Neuhaus EB, Dugan VG, Wentworth DE, Barnes JR. 2018. Direct RNA Sequencing of the Coding Complete Influenza A Virus Genome. Scientific Reports 8:14408.

34. Vella M. 2023. Nanoporetech Dorado. DOI: https://github.com/nanoporetech/dorado Accessed July 26, 2023.

35. Wu W, Zhang W, Booth JL, Hutchings DC, Wang X, White VL, Youness H, Cross CD, Zou M-H, Burian D, Metcalf JP. 2016. Human primary airway epithelial cells isolated from active smokers have epigenetically impaired antiviral responses. Respiratory Research 17:111.

36. Wick RR, Judd LM, Holt KE. 2019. Performance of neural network basecalling tools for Oxford Nanopore sequencing. Genome biology 20:129-129.

37. Li H. 2018. Minimap2: pairwise alignment for nucleotide sequences. Bioinformatics 34:3094-3100.

38. GENCODE 45 human GRCh38.p14. https://www.gencodegenes.org/human/. Accessed March 23, 2023.

39. Tang AD, Soulette CM, van Baren MJ, Hart K, Hrabeta-Robinson E, Wu CJ, Brooks AN. 2020. Full-length transcript characterization of SF3B1 mutation in chronic lymphocytic leukemia reveals downregulation of retained introns. Nature Communications 11:1438.

40. Huang S, Wylder AC, Pan T. 2024. Simultaneous nanopore profiling of mRNA m(6)A and pseudouridine reveals translation coordination. Nat Biotechnol doi:10.1038/s41587-024-02135-0.

41. Love MI, Huber W, Anders S. 2014. Moderated estimation of fold change and dispersion for RNA-seq data with DESeq2. Genome Biology 15:550.

42. Steuerman Y, Cohen M, Peshes-Yaloz N, Valadarsky L, Cohn O, David E, Frishberg A, Mayo L, Bacharach E, Amit I, Gat-Viks I. 2018. Dissection of Influenza Infection In Vivo by Single-Cell RNA Sequencing. Cell Syst 6:679-691.e4.

43. Sun J, Vera JC, Drnevich J, Lin YT, Ke R, Brooke CB. 2020. Single cell heterogeneity in influenza A virus gene expression shapes the innate antiviral response to infection. PLoS Pathog 16:e1008671.

44. Joshua JCM, Gilles V, Anna D-G, Steven PC, Sam A, Matthew FF, Danya T, Amir R, Peiyao W, Ashley B, Pamela S, Mathieu M, Rodrigo J-S, Spencer DR, Arata T, Diana Z, Warren LL, Carl DR, Matthew SM, Kjetil A, Wolfgang MK, Jeremy AS, Martin RS. 2022. Cigarette smoke augments CSF3 expression in neutrophils to compromise alveolar–capillary barrier function during influenza infection. European Respiratory Journal 60:2102049.

45. Lichinchi G, Zhao BS, Wu Y, Lu Z, Qin Y, He C, Rana TM. 2016. Dynamics of Human and Viral RNA Methylation during Zika Virus Infection. Cell Host Microbe 20:666-673.

46. Jiang J, Lu Y, Zhang F, Pan T, Zhang Z, Wan Y, Ren X, Zhang R. 2022. Semaphorin 4B promotes tumor progression and associates with immune infiltrates in lung adenocarcinoma. BMC Cancer 22:632.

47. Zhou J, Wan J, Gao X, Zhang X, Jaffrey SR, Qian SB. 2015. Dynamic m(6)A mRNA methylation directs translational control of heat shock response. Nature 526:591-4.

48. Zhang X, Yu W. 2022. Heat shock proteins and viral infection. Frontiers in Immunology 13.

49. Thompson MG, Dittmar M, Mallory MJ, Bhat P, Ferretti MB, Fontoura BMA, Cherry S, Lynch KW. 2020. Viral-induced alternative splicing of host genes promotes influenza replication. eLife 9:e55500.

50. Munk M, Villalobo E, Villalobo A, Berchtold MW. 2022. Differential expression of the three independent CaM genes coding for an identical protein: Potential relevance of distinct mRNA stability by different codon usage. Cell Calcium 107:102656.

51. Rom A, Melamed L, Gil N, Goldrich MJ, Kadir R, Golan M, Biton I, Perry RB-T, Ulitsky I. 2019. Regulation of CHD2 expression by the Chaserr long noncoding RNA gene is essential for viability. Nature Communications 10:5092.

52. Liu J, Zhan Y, Wang J, Wang J, Guo J, Kong D. 2020. Long noncoding RNA LINC01578 drives colon cancer metastasis through a positive feedback loop with the NF-κB/YY1 axis. Mol Oncol 14:3211-3233.

53. Profumo V, Forte B, Percio S, Rotundo F, Doldi V, Ferrari E, Fenderico N, Dugo M, Romagnoli D, Benelli M, Valdagni R, Dolfini D, Zaffaroni N, Gandellini P. 2019. LEADeR role of miR-205 host gene as long noncoding RNA in prostate basal cell differentiation. Nature Communications 10:307.

54. Bezzecchi E, Pagani G, Forte B, Percio S, Zaffaroni N, Dolfini D, Gandellini P. 2022. MIR205HG/LEADR Long Noncoding RNA Binds to Primed Proximal Regulatory Regions in Prostate Basal Cells Through a Triplex- and Alu-Mediated Mechanism. Front Cell Dev Biol 10:909097.

55. Papac-Milicevic N, Breuss JM, Zaujec J, Ryban L, Plyushch T, Wagner GA, Fenzl S, Dremsek P, Cabaravdic M, Steiner M, Glass CK, Binder CJ, Uhrin P, Binder BR. 2012. The Interferon Stimulated Gene 12 Inactivates Vasculoprotective Functions of NR4A Nuclear Receptors. Circulation Research 110:e50-e63.

56. Martin FJ, Amode MR, Aneja A, Austine-Orimoloye O, Azov Andrey G, Barnes I, Becker A, Bennett R, Berry A, Bhai J, Bhurji Simarpreet K, Bignell A, Boddu S, Branco Lins PR, Brooks L, Ramaraju SB, Charkhchi M, Cockburn A, Da Rin Fiorretto L, Davidson C, Dodiya K, Donaldson S, El Houdaigui B, El Naboulsi T, Fatima R, Giron CG, Genez T, Ghattaoraya GS, Martinez JG, Guijarro C, Hardy M, Hollis Z, Hourlier T, Hunt T, Kay M, Kaykala V, Le T, Lemos D, Marques-Coelho D, Marugán JC, Merino Gabriela A, Mirabueno Louisse P, Mushtaq A, Hossain Syed N, Ogeh DN, Sakthivel MP, Parker A, Perry M, Piližota I, Prosovetskaia I, et al. 2023. Ensembl 2023. Nucleic Acids Research 51:D933-D941.

57. Zhang Y, Zhang L-S, Dai Q, Chen P, Lu M, Kairis EL, Murugaiah V, Xu J, Shukla RK, Liang X, Zou Z, Cormet-Boyaka E, Qiu J, Peeples ME, Sharma A, He C, Li J. 2022. 5-methylcytosine (m⁵C) RNA modification controls the innate immune response to virus infection by regulating type I interferons. Proceedings of the National Academy of Sciences 119:e2123338119.

58. Warda AS, Kretschmer J, Hackert P, Lenz C, Urlaub H, Höbartner C, Sloan KE, Bohnsack MT. 2017. Human METTL16 is a N(6)-methyladenosine (m(6)A) methyltransferase that targets pre-mRNAs and various non-coding RNAs. EMBO Rep 18:2004-2014.

59. Gu W, Gallagher GR, Dai W, Liu P, Li R, Trombly MI, Gammon DB, Mello CC, Wang JP, Finberg RW. 2015. Influenza A virus preferentially snatches noncoding RNA caps. Rna 21:2067-75.

60. Koppstein D, Ashour J, Bartel DP. 2015. Sequencing the cap-snatching repertoire of H1N1 influenza provides insight into the mechanism of viral transcription initiation. Nucleic Acids Res 43:5052-64.

61. Sikora D, Rocheleau L, Brown EG, Pelchat M. 2014. Deep sequencing reveals the eight facets of the influenza A/HongKong/1/1968 (H3N2) virus cap-snatching process. Sci Rep 4:6181.

62. Gultyaev AP, Spronken MI, Funk M, Fouchier RAM, Richard M. 2021. Insertions of codons encoding basic amino acids in H7 hemagglutinins of influenza A viruses occur by recombination with RNA at hotspots near snoRNA binding sites. Rna 27:123-132.

63. Taoka M, Nobe Y, Yamaki Y, Sato K, Ishikawa H, Izumikawa K, Yamauchi Y, Hirota K, Nakayama H, Takahashi N, Isobe T. 2018. Landscape of the complete RNA chemical modifications in the human 80S ribosome. Nucleic Acids Research 46:9289-9298.

64. Chen J, Zhang K, Zhi Y, Wu Y, Chen B, Bai J, Wang X. 2021. Tumor-derived exosomal miR-19b-3p facilitates M2 macrophage polarization and exosomal

LINC00273 secretion to promote lung adenocarcinoma metastasis via Hippo pathway. Clin Transl Med 11:e478.

65. Sarkar A, Rahaman A, Biswas I, Mukherjee G, Chatterjee S, Bhattacharjee S, Mandal DP. 2020. TGFβ mediated LINC00273 upregulation sponges mir200a-3p and promotes invasion and metastasis by activating ZEB1. J Cell Physiol 235:7159-7172.

66. Haynes W. 2013. Benjamini–Hochberg Method, p 78-78. *In* Dubitzky W, Wolkenhauer O, Cho K-H, Yokota H (ed), Encyclopedia of Systems Biology doi:10.1007/978-1-4419-9863-7_1215. Springer New York, New York, NY.

67. Martin FJ, Amode MR, Aneja A, Austine-Orimoloye O, Azov Andrey G, Barnes I, Becker A, Bennett R, Berry A, Bhai J, Bhurji Simarpreet K, Bignell A, Boddu S, Branco Lins PR, Brooks L, Ramaraju SB, Charkhchi M, Cockburn A, Da Rin Fiorretto L, Davidson C, Dodiya K, Donaldson S, El Houdaigui B, El Naboulsi T, Fatima R, Giron CG, Genez T, Ghattaoraya GS, Martinez JG, Guijarro C, Hardy M, Hollis Z, Hourlier T, Hunt T, Kay M, Kaykala V, Le T, Lemos D, Marques-Coelho D, Marugán JC, Merino Gabriela A, Mirabueno Louisse P, Mushtaq A, Hossain Syed N, Ogeh DN, Sakthivel MP, Parker A, Perry M, Piližota I, Prosovetskaia I, et al. 2022. Ensembl 2023. Nucleic Acids Research 51:D933-D941.

68. Huang S, Wylder AC, Pan T. 2024. Simultaneous nanopore profiling of mRNA m6A and pseudouridine reveals translation coordination. Nature Biotechnology doi:10.1038/s41587-024-02135-0.

69. Hofacker IL, Lorenz, R. 2014. Predicting RNA structure: advances and limitations. Methods Mol Biol 1086:1-19.